Formation and Growth of Pd Nanoparticles Inside a Highly Cross-Linked Polystyrene Support: Role of the Reducing Agent

ARTICLE *in* THE JOURNAL OF PHYSICAL CHEMISTRY C · APRIL 2014

Impact Factor: 4.77 · DOI: 10.1021/jp5003897

8 AUTHORS, INCLUDING:

Elisa Borfecchia
Università degli Studi di Torino
28 PUBLICATIONS **236** CITATIONS
SEE PROFILE

G. Portale
European Synchrotron Radiation Facility
107 PUBLICATIONS **1,199** CITATIONS
SEE PROFILE

Carlo Lamberti
Università degli Studi di Torino
382 PUBLICATIONS **13,162** CITATIONS
SEE PROFILE

THE JOURNAL OF PHYSICAL CHEMISTRY C

Article

pubs.acs.org/JPCC

Formation and Growth of Pd Nanoparticles Inside a Highly Cross-Linked Polystyrene Support: Role of the Reducing Agent

Elena Groppo,*[,†] Giovanni Agostini,[†] Elisa Borfecchia,[†] Liu Wei,[†,#] Francesco Giannici,[‡] Giuseppe Portale,[§] Alessandro Longo,*[,§,∥] and Carlo Lamberti[†,⊥,¶]

[†]Department of Chemistry, INSTM and NIS Centre, University of Torino, Via Quarello 15, I-10135 Torino, Italy

[‡]Dipartimento di Fisica e Chimica, Università di Palermo, viale delle Scienze, I-90128 Palermo, Italy

[§]Netherlands Organization for Scientific Research at ESRF, BP 220, F-38043 Grenoble Cedex 9, France

[∥]Istituto per lo Studio dei Materiali Nanostrutturati, Sezione di Palermo, Consiglio Nazionale delle Ricerche, Via La Malfa, 153, I-90146 Palermo, Italy

[⊥]CrisDI Interdepartmental Center for Crystallography, University of Torino, via P. Giuria 5, I-10125 Torino, Italy

[¶]Southern Federal University, Zorge Street 5, 344090 Rostov-on-Don, Russia

ABSTRACT: Simultaneous time-resolved SAXS and XANES techniques were employed to follow in situ the formation of Pd nanoparticles in a porous polystyrene support, using palladium acetate as a precursor and gaseous H_2 or CO as reducing agents. These results, in conjunction with data obtained by diffuse reflectance UV−vis and DRIFT spectroscopy and TEM measurements, allowed unraveling of the different roles played by gaseous H_2 and CO in the formation of the Pd nanoparticles. In particular, it was found that the reducing agent affects (i) the reduction rate (which is faster in the presence of CO) and (ii) the properties of the hosted nanoparticles, in terms of size (bigger with CO), morphology (spherical with H_2, triangular-like with CO), and surface properties (unclean with CO). The importance of a multitechnique approach in following the whole process of metal nanoparticles formation clearly emerges.

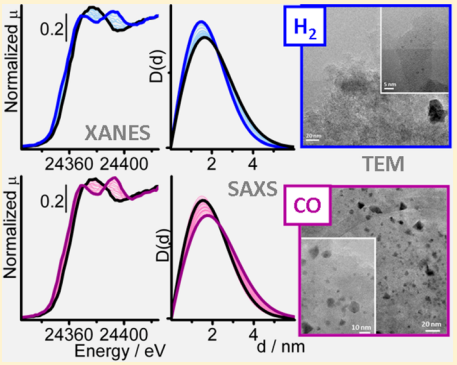

1. INTRODUCTION

Metal nanoparticles (NPs) deposited on high-surface-area supports are strategic materials in catalysis; usually they show enhanced catalytic performances compared to homogeneous catalysts, due to the fact that the particle growth and aggregation are inhibited. Among heterogeneous catalysts composed of metal NPs, those based on Pd are largely employed in a number of applications, in combination with several supports having organic (such as carbons) or inorganic (Al_2O_3, SiO_2, and others) nature.[1−7] In recent years, Pd NPs supported on porous polymers have become a promising class of catalysts because of their unique physical−chemical properties and attractive catalytic performances.[8−23] The polymer acts simultaneously as support and stabilizer, thanks to the dual effect of porosity (steric stabilization) and charged functional groups (electrostatic stabilization).[24−28] For this reason, Pd catalysts supported on polymers are more stable than the homogeneous counterparts; moreover, they are cheaper, easy to handle, and easily recovered.

Most of the preparation methods for polymer-supported Pd NPs involve the use of a weakly coordinated cationic precursor of Pd, which is impregnated onto the polymer and then reduced by means of hazardous reagents (such as hydrazine). The need for synthetic routes involving minimal reagents and mild reaction conditions was recently pointed out in order to make their industrial application feasible.[29] For this reason, in this work we explore the formation of Pd NPs starting from palladium acetate precursor inside a highly porous polymer (a cross-linked polystyrene), in the presence of H_2 or CO in the gas phase (low equilibrium pressure) as reducing agent. The structural, optical, and vibrational properties of the Pd/polymer composite before and after H_2 reduction were already characterized in our previous work,[30] but a real-time monitoring of the evolution of the Pd NPs during the reduction process was missing, and the effect of CO as reducing agent was never explored. The in situ investigation of the Pd NP formation is of great interest because it is well-known that the size and shape of metal NPs depend on the kinetics of the nucleation and growth processes.[31] Hence, understanding the phenomena behind the NP formation is fundamental in order to tune the NP properties, and therefore their catalytic performances.[32]

In order to follow in situ the reduction of the Pd acetate/polymer composite in the presence of different reducing agents in the gas phase, we have applied simultaneously time-resolved small-angle X-ray scattering (SAXS) and X-ray absorption near-edge structure (XANES) techniques. Both time-resolved SAXS[33−39] and time-resolved X-ray absorption fine structure (XAFS)[34,40] have been widely used in an independent way to measure the quantity (such as concentration or mass), the size,

Received: January 13, 2014
Revised: March 17, 2014
Published: March 22, 2014

   dx.doi.org/10.1021/jp5003897 | J. Phys. Chem. C 2014, 118, 8406−8415

and the oxidation state of metal NPs in solution as a function of time, thanks to the efficient penetration of high energy synchrotron X-rays into the liquid media. Also a few works at present concern the simultaneous application of the two techniques to follow metal NP evolution in solution as a function of time.[41,42] By contrast, time-resolved SAXS and X-ray absorption spectroscopy (XAS) techniques were rarely applied to investigate in situ the growth process of metal NPs onto solid supports in the presence of reducing agents in the gas phase[43−47] and, to the best of our knowledge, there are no examples in the literature of simultaneous in situ SAXS−XAS techniques applied to this purpose. On the basis of our previous experience on the importance of a multitechnique approach in the investigation of Pd NPs,[7,30,48−52] SAXS and XAS have been applied in conjunction with laboratory in situ techniques such as diffuse reflectance UV−vis (DR UV−vis) spectroscopy, diffuse reflectance IR spectroscopy (DRIFT), and transmission electron microscopy (TEM). Particular attention is devoted to the investigation of the different roles played by gaseous H_2 and CO in affecting the reduction rate as well as the properties of the obtained Pd NPs in terms of particle size and morphology.

2. EXPERIMENTAL SECTION

2.1. Preparation of Polymer-Supported Pd NPs. Poly(4-ethylstyrene-*co*-divinylbenzene) (Aldrich) was used as a support for Pd nanoparticles. A sketch of the polymer is reported in Scheme 1.

Scheme 1

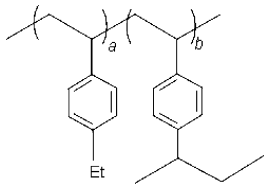

The 25% cross-linking with divinylbenzene (DVB) guarantees a high surface area (1000 $m^2\ g^{-1}$) due to the contemporaneous presence of micropores (1−2 nm) and mesopores (2−50 nm).[30,53] The starting Pd(II)−polymer composite was prepared by impregnation, stirring the polymer with an appropriate amount of palladium acetate in acetonitrile, resulting in a final Pd loading of 10 wt %.[30] After impregnation, the sample was filtered and dried at room temperature. We demonstrated previously that the palladium acetate precursor is incorporated into the polymer scaffold by retaining the trimeric structure characteristic of the bulk phase. In the absence of any functional group in the polymer, no chemical reaction occurs between the palladium acetate and the polymer.[30]

In situ reduction of the Pd(II)−polymer to get Pd(0)-containing polymer was carried out in mild conditions in the presence of different reducing agents (H_2 and CO) in the gas phase. The reduction process was conducted in either dynamic or static conditions, depending on the experimental setup available for the different techniques employed for the in situ characterization. We notice that reduction is accomplished at low H_2 (or CO) equilibrium pressures. Further details are given in section 2.2.

2.2. Characterization Techniques. All the Pd-containing polymers were characterized in the powder state by a combination of experimental techniques. When possible, the reduction of Pd(II)−polymer into Pd(0)−polymer was monitored in situ, i.e., during the thermal treatment at increasing temperature in the presence of the reducing agent in the gas phase.

2.2.1. Diffuse Reflectance UV−Vis Spectroscopy. UV−vis spectra were collected in reflectance mode on a Varian Cary5000 instrument equipped with a reflectance sphere. The samples were measured in the form of powder in a devoted cell equipped with a bulb in optical quartz (suprasil), which allows thermal treatments to be performed, both in vacuum and in the presence of gases (in the 10^{-4}−800 mbar range). The Pd(II)−polymer sample was measured in the fresh form and after prolonged degassing at room temperature. The subsequent in situ reduction procedure was performed in static conditions and consisted of the following steps: (i) interaction with the reducing agent (equilibrium pressure of about 100 mbar) at room temperature for 1 h; (ii) heating at a rate of 1 °C/min up to 60 °C and waiting at that temperature for 1 h; (iii) heating at a rate of 1 °C/min up to 120 °C and waiting at that temperature for 1 h. A UV−vis spectrum was collected after each step.

2.2.2. Fourier Transform Infrared (FT-IR) Spectroscopy. FT-IR spectra were collected in reflectance mode (DRIFT) on a Nicolet 6700 instrument, equipped with a MCT detector. A Thermo Fisher Environmental Chamber was adopted to record FT-IR spectra in reaction conditions. The Pd(II)−polymer sample was first degassed in a dynamic vacuum at room temperature down to 10^{-3} mbar. Successively, the sample was contacted with the reducing agent at room temperature (equilibrium pressure of about 100 mbar) for 30 min, and then heated in the presence of the reducing agent (H_2 or CO) up to 160 °C, at a heating rate of 2 °C/min, and mantained at 160 °C for 1 h. FT-IR spectra were recorded at regular time intervals during the whole reduction process. Finally, the cell was degassed at 160 °C, and the temperature was brought down to room temperature.

In order to characterize the surface properties of the resulting Pd NPs, carbon monoxide was used as a probe, following a widely applied procedure as reported elsewhere.[49,51,54−60] Briefly, the Pd(0)-containing polymers were contacted in situ with CO (equilibrium pressure P_{CO} = 50 mbar) and a FT-IR spectrum was collected. P_{CO} was then gradually decreased stepwise from 50 to 10^{-3} mbar, and the corresponding FT-IR spectra were recorded. The final FT-IR spectrum corresponds to CO species irreversibly adsorbed at room temperature. All the IR spectra have been converted from reflectance to Kubelka−Munk (K.M.) values.

2.2.3. Transmission Electron Microscopy. Transmission electron micrographs were obtained using a JEOL 3010-UHR instrument operating at 300 kV, equipped with a 2k × 2k pixel Gatan US1000 CCD camera. Samples were deposited on a copper grid covered with a lacey carbon film.

2.2.3. XAS−SAXS. In situ XAS and SAXS measurements were carried out simultaneously on the BM26A beamline at the ESRF facility (Grenoble, France), using the experimental setup previously reported.[61,62] The powdered samples were placed in a 2 mm glass capillary connected to gas flow, either CO (5%)/He or H_2 (5%)/He at 25 mL/min. During each reduction treatment, the temperature of the capillary was raised from 25 to 200 °C using a heat gun, at a heating rate of 2 °C/min.

Fluorescence XAS spectra at the Pd K-edge (24.3 keV) were collected with a nine-element Ge detector. The energy delivered by the double crystal Si(111) monochromator was calibrated measuring the XANES spectrum of a palladium foil in transmission mode. The spectra were normalized and treated with Athena software.[63] The SAXS patterns were collected

dx.doi.org/10.1021/jp5003897 | J. Phys. Chem. C 2014, 118, 8406−8415

using a 2D Mar detector. The sample−detector distance was calibrated with standard Ag behenate. The energy change between the start and the end of the XAS spectrum (about 120 eV) is irrelevant to SAXS, so the incident beam wavelength can be treated as constant, $\lambda = 0.509(1)$ Å. The resulting q-range was 0.5−7 nm^{-1} ($q = 4\pi \sin\theta/\lambda$, where θ is the X-ray scattering angle), allowing investigation of the 12.5−0.9 nm d-spacing interval. Each XAS spectrum was collected in about 300 s. As the readout and erasing time of the 2D Mar detector was 180 s, each XAS spectrum was collected with an integration time of 120 s; in such a way we obtained a 1 to 1 correspondence between XAS spectra and SAXS patterns. The patterns were integrated with Fit2D and modeled using a homemade code.[64]

3. RESULTS AND DISCUSSION

3.1. Reactivity of Pd(II)−Polymer toward H_2 and CO As Monitored by UV−Vis Spectroscopy. As anticipated, the routes usually described in the literature to prepare supported metal NPs use organic solvents, hazardous reagents (such as $NaBH_4$ or hydrazine), stabilizing agents, or harsh conditions.[65−67] Herein, we turned our attention toward a reduction route involving minimal reagents and mild conditions (in terms of temperature and pressure). Among the simplest reducing agents we selected H_2 and CO gases. It is generally accepted that palladium acetate is reduced by H_2 according to the overall chemical eq 1: the reaction is stoichiometric and acetic acid is the only byproduct.

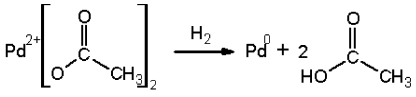

(1)

The reaction of palladium acetate with CO is less established and strongly depends on the conditions at which it is carried out. It has been reported that palladium acetate in glacial acetic acid is carbonylated at 323 K in the presence of CO (P_{CO} = 1 atm) according to reaction 2, to give yellow crystals of the $Pd_4(\mu\text{-}CO)_4(\mu\text{-}OAc)_4$ complex, in which Pd is formally in the +1 oxidation state; acetic anhydride is the main byproduct.[68,69] The formation of other polynuclear Pd(+1) carbonyl carboxylates was also reported in the literature,[70−73] as well as the complete reduction of palladium acetate to Pd(0) by CO in organic solutions, involving the formation of CO_2 as a byproduct, as described in eq 3.[68]

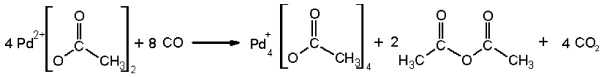

(2)

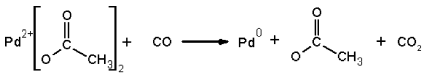

(3)

In the Pd(II)−polymer sample investigated herein, palladium acetate is highly dispersed in the polymer matrix, which can act as a stabilizer, as well as a templating agent, for Pd-based clusters. The interaction of palladium acetate with the polymer is expected to affect the chemistry of the Pd complex. For example, both the reducibility of supported palladium acetate and the final products could be different from that observed for palladium acetate in solution. The reactivity of the Pd(II)−polymer toward H_2 and CO at increasing temperature is testified by the observation that the color of the sample gradually turns from orange to dark brown, indicating that the Pd(II)−polymer is converted into Pd(0)−polymer. To confirm the formation of Pd nanoparticles, diffuse reflectance UV−vis measurements were performed. Figure 1 shows the DR UV−vis spectra of fresh Pd(II)−polymer (black spectra) and of the same sample after thermal treatment in the presence of H_2 (Figure 1a) and CO (Figure 1b) at different temperatures, up

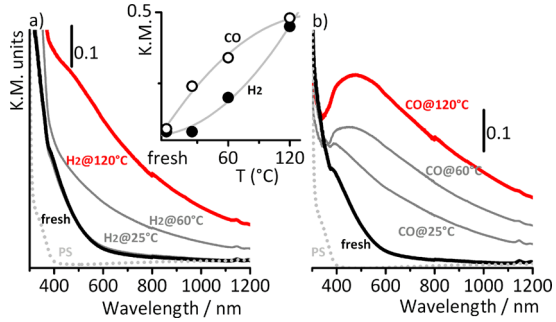

Figure 1. DR UV−vis spectra of fresh Pd(II)−polymer (black) and of the same sample reduced in (a) H_2 or (b) CO at progressively higher temperature up to 120 °C (red); heating ramp 1 °C/min. Also the spectrum of pure polymer is shown for comparison (dotted gray). K.M. = Kubelka−Munk units. The inset reports the intensity of each UV−vis spectrum taken at 500 nm; filled and open circles refer to Pd(II)−polymer reduced in H_2 and CO, respectively.

to 120 °C (red spectra); the spectrum of the pure polymer is reported for comparison (dotted gray). The UV−vis spectrum of the fresh sample is dominated by a broad absorption band centered around 360 nm, having a pronounced tail extending down to 600 nm. This absorption band is characteristic of the palladium acetate precursor and is assigned to a ligand-to-metal charge transfer transition from the acetate ligands to the Pd(II) ions.[74,75] The UV−vis spectrum of Pd(II)−polymer does not change after exposure of the sample to H_2 at room temperature, even after 1 h of waiting (Figure 1a). On the contrary, an evident change is observed after the same time of exposure to CO at room temperature (Figure 1b). These data suggest that the activation energy for reduction of Pd(II)−polymer is lower in the presence of CO than of H_2.

Upon heating Pd(II)−polymer in the presence of both H_2 and CO, the growth of an almost featureless absorption band in the visible range is observed, which indicates the formation of Pd nanoparticles.[76,77] This absorption is related to the excitation of the surface plasmon resonance (i.e., coherent oscillation of the conduction band electrons induced by the interacting electromagnetic fields) that, for Pd nanoparticles,[78] is much less defined than for other metals such as Cu, Ag, and Au.[79,80] The intensity of the UV−vis spectra evaluated at 500 nm is plotted as a function of the reduction temperature in the inset of Figure 1, for both H_2 and CO reducing agents. It is evident that Pd(II)−polymer is reduced at a lower temperature by CO than by H_2. Moreover, the two final spectra (obtained after heating at 120 °C in the presence of the reducing agent, red spectra in Figure 1) are quite different. In particular, the spectrum of the Pd(0)−polymer obtained in the presence of CO shows a well-defined maximum at 500 nm, whereas a much broader spectrum is observed for Pd(0)−polymer obtained in the presence of H_2.

The UV−vis data shown in Figure 1 provide clear evidence that both H_2 and CO convert the Pd(II)−polymer into Pd(0)−polymer; however, the reduction rate and the properties of the final Pd NPs are affected by the reducing agent. In order to get further insights into the mechanism of Pd(II)−polymer reduction, we performed a series of measurements in reaction conditions by means of FT-IR spectroscopy and simultaneous SAXS−XAS techniques, coupled with ex situ TEM analysis.

dx.doi.org/10.1021/jp5003897 | J. Phys. Chem. C 2014, 118, 8406−8415

The results obtained in the presence of H_2 will be discussed at first, followed by those obtained in the presence of CO.

3.2. Reduction of Pd(II)−Polymer by H_2 Followed in Reaction Conditions. *3.2.1. DRIFT Spectroscopy in Reaction Conditions and ex Situ TEM.* The FT-IR spectrum of fresh Pd(II)−polymer is shown in Figure 2 (black) in comparison to

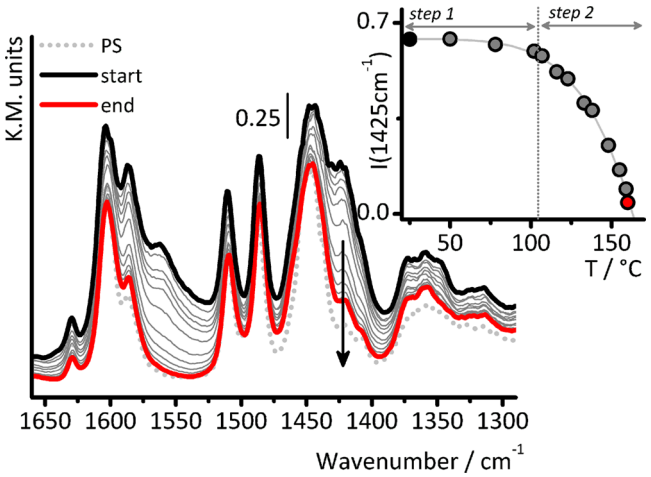

Figure 2. DRIFT spectra collected during reduction of Pd(II)−polymer in H_2 from room temperature (black) to 160 °C (red); heating rate 2 °C/min. Also the spectrum of pure polymer is shown for comparison (dotted gray). The spectra are shown in the 1700−1300 cm^{-1} region, where the most intense IR absorption bands characteristic of the acetate groups are observed. The inset shows the evolution of the intensity of the IR absorption band at 1425 cm^{-1} as a function of temperature (black arrow in the main part).

that of pure polymer (dotted gray) in the 1700−1300 cm^{-1} region, which contains the characteristic absorption bands due to the acetate ligand. No changes are observed in the vibrational modes of the hosting polymer after the introduction of the palladium acetate precursor, but only the appearance of a few additional IR absorption bands due to the vibrational modes of the acetate groups. In particular, the strong IR absorption bands around 1570 and 1425 cm^{-1} are assigned to υ_{as}(COO) and υ_s(COO) of trimeric palladium acetate.[81−83]

The IR spectrum of Pd(II)−polymer does not change in the presence of H_2 at room temperature (in agreement with UV−vis data), whereas the IR absorption bands characteristic of the acetate groups gradually decrease in intensity upon heating of the sample in the presence of H_2 (gray spectra in Figure 2), up to disappearing at 160 °C (red spectrum in Figure 2). The intensity of the IR absorption band at 1425 cm^{-1} (characteristic of the acetate groups) is reported as a function of the temperature in the inset of Figure 2. It is evident that reduction of Pd(II)−polymer occurs in two main steps: at lower temperature the reduction rate is quite slow (step 1 in the inset of Figure 2), whereas at higher temperature reduction proceeds faster (step 2 in the inset of Figure 2). As previously observed, a complete removal of the acetate groups is achieved at 160 °C (compare the red and the dotted gray spectra). The data shown in Figure 2 provide evidence that palladium acetate is reduced by H_2 according to the overall chemical reaction, eq 1; the byproduct (acetic acid) is likely desorbed at the reaction temperature and hence it is not detectable by FT-IR spectroscopy. It is important to notice that full reduction is obtained at lower temperature (120 °C) when a slower heating rate (1 °C/min) is employed, in agreement with UV−vis results (i.e., the heating rate influences the speed of palladium acetate reduction).

The properties of the Pd nanoparticles obtained at the end of the reduction process monitored by FT-IR spectroscopy (data shown in Figure 2) were investigated by means of (i) TEM, which gives direct evidence of the shape and dimension of the Pd nanoparticles, and (ii) FT-IR spectroscopy of adsorbed CO, which offers information on the surface properties of the metal nanoparticles.[49,51,54−60] Figure 3a displays representative TEM

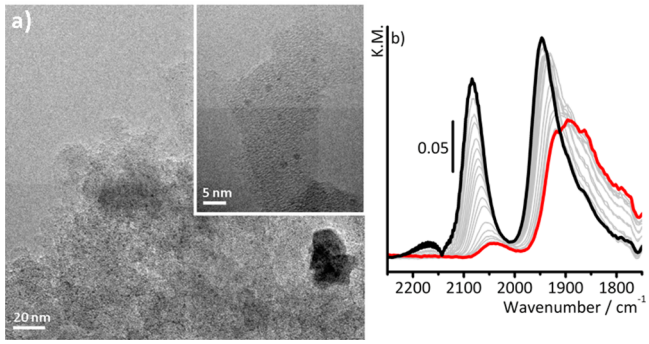

Figure 3. (a) Representative TEM images of Pd particles obtained after reduction of Pd(II)−polymer in H_2 at a heating rate of 2 °C/min up to 160 °C. (b) Background subtracted FT-IR spectra (collected in reflectance mode) of CO adsorbed at room temperature on the same sample. The sequence of FT-IR spectra shows the effect of decreasing P_{CO}, from 50 mbar (black spectrum) to 10^{-3} mbar (red).

images of the Pd(0)−polymer sample obtained at the end of the experiment shown in Figure 2. Very small Pd nanoparticles with a spherical shape and a homogeneous size are observed; most of them have a diameter smaller than 2 nm and are hardly detectable by our TEM instrument. In some regions of the sample a few bigger particles (larger than 15 nm) were also detected (an example is shown in Figure 3a). It is important to observe that (i) the big particles are rare, hence they do not affect the DRIFT results that probe the surface Pd atoms only, and (ii) these particles cannot be observed by SAXS, because the $2\theta_{min}$ (hence the q_{min}) was too high, resulting in a d_{max} cutoff at 12.5 nm. On the contrary, even a small number of large particles have a strong influence on the XAS data,[51] as it will be discussed later.

Figure 3b shows the background subtracted FT-IR spectra of CO adsorbed at room temperature on the same sample observed by TEM, as a function of the CO coverage. The IR spectrum collected at the highest CO coverage (bold black) is characterized by two main absorption bands at 2081 and 1944 cm^{-1}, which are assigned to linear (terminal) and bridged carbonyl species, respectively.[54−56] The two absorption bands have similar intensities. It was previously demonstrated that the relative proportion of linear and bridged adsorbed carbonyls correlates with the size and the surface regularity of the Pd particles. In particular, small and amorphous metal particles exhibit prevalently linear CO species, whereas an increase in the particle size results in a greater number of bridged carbonyls.[30,54,57,84−86] Therefore, the spectra in Figure 3b suggest that the Pd particles obtained by reduction of Pd(II)−polymer in H_2 present a high level of defectivity. The adsorbed carbonyls are easily reversible upon degassing at room temperature (from gray to red spectra). The absorption bands due to linear and bridged carbonyls decrease in intensity and gradually downward shift upon lowering of the CO coverage. The easy

dx.doi.org/10.1021/jp5003897 | J. Phys. Chem. C 2014, 118, 8406−8415

reversibility of adsorbed CO reveals that the polymeric support plays an "active" role and competes with CO in interacting with Pd nanoparticles.[30,87]

Pd(0)−polymer samples obtained by reducing Pd(II)−polymer in H_2 at a different heating rate are very similar in terms of particle shape and size, as well as in terms of exposed surface sites and defectivity. Therefore, it can be stated that the heating rate affects the speed of Pd(II)−polymer reduction, but not the final properties of the obtained Pd nanoparticles.

3.2.2. Simultaneous SAXS−XAS Experiment in Reaction Conditions. Simultaneous SAXS and XAS techniques were simultaneously applied to get combined information on the evolution of the Pd oxidation state, the size of the formed Pd NPs, and the quantity of Pd contributing to the total scattering as a function of both time and temperature. A summary of the results is shown in Figure 4. In particular, Figure 4a,e shows the

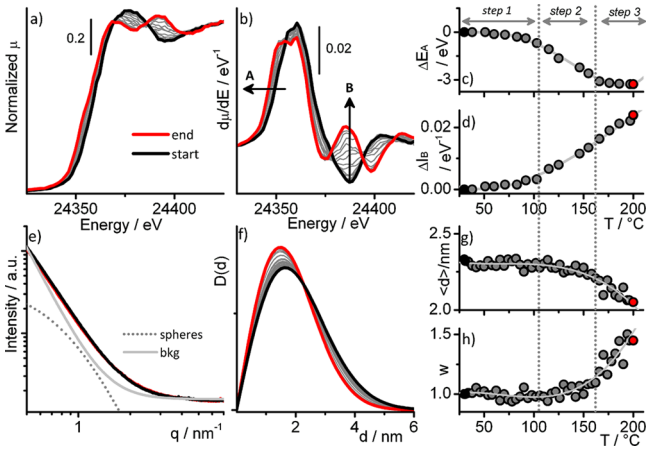

Figure 4. SAXS−XAS data collected simultaneously during reduction of Pd(II)−polymer in H_2 from room temperature (black) to 200 °C (red); heating rate 2 °C/min. (a and b) Evolution of the normalized XANES spectra and of the derivative signal. Parts (c) and (d) show the evolution as a function of temperature of features A (shift in energy) and B (change in intensity) of the derivative XANES spectra (see arrows in part b). (e) SAXS patterns at the beginning (black) and the end (red) of the temperature ramp. Also an example of the theoretical signals obtained by considering a distribution of spherical particles (dotted gray) and the background (gray) are reported. (f) Particle size distribution, (g) average diameter of the Pd particles, and (h) relative weight as a function of temperature, respectively, as obtained from the spherical model fitting of the SAXS data.

evolution of XANES spectra and SAXS patterns at the Pd K-edge, collected simultaneously during thermal treatment of Pd(II)−polymer in H_2 from room temperature (black) to 160 °C (red). Figure 4b shows the derivative of the XANES spectra; the evolution of the A and B features is displayed in Figure 4c,d. Figure 4f shows the particle size distribution as determined by the analysis of SAXS data, whereas Figure 4g,h reports the evolution of the mean metal cluster dimension and its relative amount with respect to the background obtained by the analysis of the SAXS data.

During the thermal reduction of Pd(II)−polymer in H_2, the XANES spectra (Figure 4a) evolve clearly from that characteristic of palladium acetate in the fresh sample (black spectrum) to a spectrum characteristic of Pd(0) at the end of the heating ramp (red spectrum).[30] The edge gradually shifts toward lower energy (down to the Pd metal value) and the white line decreases in intensity. Simultaneously, the appearance of three isosbestic points at 24 369, 24 386, and 24 404 eV testifies that Pd(II) species are transformed into Pd(0) ones. Formation of Pd NPs is further demonstrated by the growth of the band at 24 393 eV, which is the first EXAFS oscillation of Pd atoms arranged in a fcc local structure.[30] The evolution of the XANES spectra is better appreciated by looking at the derivative curves (Figure 4b). Figure 4c,d reports the evolution of features A and B as a function of the temperature. A shift in the energy position of feature A is correlated with an energy shift of the edge and therefore to a change in the oxidation state of Pd species. The energy position of feature A changes very slowly below about 100 °C (step 1), whereas a faster change is observed in the 100−160 °C range (step 2). No further changes in the position of feature A are observed above 160 °C (step 3 in Figure 4c). These data are in fair agreement with the FT-IR ones shown in Figure 2, and they confirm that (i) Pd(II)−polymer heated in the presence of H_2 is completely reduced to Pd(0)−polymer around 160 °C and (ii) the reduction process is slower in a first induction period (below 100 °C), whereas it proceeds faster above about 100 °C. The disappearance of the IR absorption bands assigned to the acetate groups (Figure 2) correlates well with the reduction of Pd(II) to Pd(0) observed by XANES.

The change in intensity of feature B corresponds to a change in the slope of the XANES spectra at the isosbestic point at 24 386 eV. As summarized in Figure 4d, feature B grows in intensity upon increasing temperature. Also in this case the reduction step is slower below about 100 °C (i.e., an induction period is observed), and then it proceeds faster at higher temperatures. Also the growth of feature B monitors the conversion of Pd(II)−polymer into Pd(0)−polymer. In addition, the intensity of B contains also information on the particle size of the formed Pd NPs, because the first EXAFS oscillation is intrinsically influenced by the relative ratio of Pd atoms on the surface and in the bulk. However, decoupling of the two pieces of information is very difficult. In this regard, it is important to observe that XANES data are averaged over all the Pd atoms contained in the sample. Since large particles contribute to feature B much more than small particles (due to the number of atoms scaling as the third power of size), the constant increase of feature B with temperature could reflect the growth of a few, larger, particles in the sample (as detected by TEM).

Complementary information on the Pd particle size can be obtained by the analysis of the SAXS data collected simultaneously to the XANES spectra. Figure 4e shows the $I(q)$ vs scattering vector q in the logarithmic scale of Pd−polymer at the beginning (black) and at the end (red) of the heating ramp in H_2. The two SAXS patterns look very similar because they are dominated by the scattering of the porous polymer. Superimposed to the experimental patterns, two additional curves are reported: (i) the background (light gray), modeled with a Porod function of the type $A + B/q^4$, with A and B constants, and (ii) the theoretical signal obtained by considering a distribution of spherical particles in decoupling approximation (dotted line). It is worth noticing that it was not possible to use the SAXS curve of the pure polymer as a background, because the introduction of palladium acetate affects the overall scattering properties. However, a blank experiment was performed to exclude that the polymer itself is modified during the heating ramp in H_2; the SAXS profiles of the bare polymer do not change, thus confirming that all the changes observed during the experiment performed on Pd(II)−polymer are due to the Pd phase. The relevant structural parameters deduced from the modeling of the SAXS data are shown in Figure 4g,h as a

dx.doi.org/10.1021/jp5003897 | J. Phys. Chem. C 2014, 118, 8406−8415

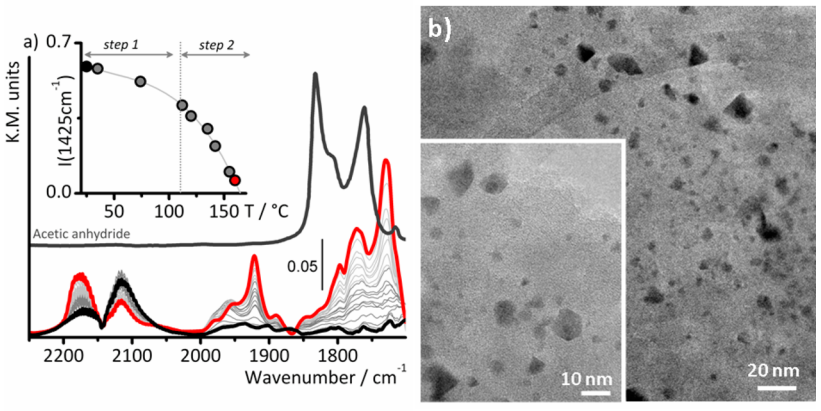

Figure 5. (a) DRIFT spectra collected during reduction of Pd(II)−polymer in CO from room temperature (black) to 160 °C (red); heating rate 2 °C/min. The spectra are shown in the 2250−1700 cm^{-1} region, where the IR absorption bands characteristic of metal carbonyl species and of C═O-containing byproducts appear. The IR spectrum of acetic anhydride is shown for comparison (vertically translated for clarity). The inset shows the evolution of the intensity of the IR absorption band at 1425 cm^{-1} (characteristic of the acetate groups) as a function of reduction temperature (spectra not shown in that interval range). (b) Representative TEM images of the Pd particles obtained at the end of the IR experiment shown in part (a).

function of the reduction temperature. Figure 4g shows the evolution of the average particle diameter; the corresponding size distributions are shown in Figure 4f. Finally, Figure 4h shows the contribution of the spherical particles with respect to the modeled background. At the beginning, the spherical particles contributing to the $I(q)$ signal are composed of palladium acetate; their average diameter is 2.3 ± 0.2 nm and the particle size distribution is quite broad. It is evident that during the induction period (i.e., below about 100 °C) both the average diameter and the number of Pd particles contributing to the total scattering remain constant. Above 100 °C a gradual decrease in the average particle size, a narrowing in the particle size distribution, and an increase in the number of particles contributing to the SAXS signal are observed. At the end of the heating ramp, Pd nanoparticles having an average diameter of 2.0 ± 0.2 nm are obtained, in fair agreement with the TEM results shown in Figure 3a. The relatively small changes undergone by the SAXS curves during the heating ramp suggest that reduction of palladium acetate in the polymer occurs without modifying the polymer cavities in which it takes place. An average shrinking of the original Pd-based particles is observed, in agreement with the higher density of metal Pd with respect to palladium acetate. It is important to observe that the few big particles (diameter larger than 10 nm) observed by TEM (and mainly contributing to the increase of feature B in the XANES spectra) could not be detected by SAXS in the available q range. Therefore, SAXS data refer only to the majority of small Pd nanoparticles having a quite homogeneous size distribution and hardly detected by TEM. In this sense, SAXS is a necessary complement to TEM characterization.

3.3. Reduction of Pd(II)−Polymer by CO Followed in Reaction Conditions. *3.3.1. DRIFT Spectroscopy in Reaction Conditions and ex Situ TEM.* The same set of experiments discussed in section 3.2 were performed during transformation of Pd(II)−polymer into Pd(0)−polymer using CO as reducing agent. At first, the reduction of palladium acetate in the presence of CO was monitored as a function of temperature by means of FT-IR spectroscopy in reflectance mode. Oppositely to what is observed in the presence of H_2 and in agreement with the UV−vis data shown in Figure 1, the IR spectrum of Pd(II)−polymer starts to change in the presence of CO already at room temperature. The decrease in intensity of the IR absorption band at 1425 cm^{-1} (characteristic of acetate groups) as a function of temperature is reported in the inset of Figure 5a. Also in this case reduction of Pd(II)−polymer is quite slow during step 1, whereas at higher temperature reduction proceeds faster. An almost complete reduction is achieved at 160 °C.

The FT-IR experiment performed in the presence of CO gives additional information. As a matter of fact, CO may not only act as a reducing agent, but also as a stabilizer of the partially reduced Pd clusters (see section 3.1), and as a probe for the surface properties of the formed Pd NPs. Therefore, it is of particular interest to look at the FT-IR spectra not only in the 1700−1300 cm^{-1} region, but also in the 2200−1700 cm^{-1} region, where carbonyl species give their contributions (Figure 5a). The IR spectrum at the beginning of the heating ramp (black) shows a broad absorption band at 2115 cm^{-1}, assigned to CO adsorbed on Pd(II) species (likely, a few defect sites in palladium acetate particles).[88−93] This band decreases in intensity upon increasing temperature, without completely disappearing. Simultaneously, a complex series of IR absorption bands appear in two main regions: (i) 2000−1900 cm^{-1}, typical of metal carbonyls, and (ii) 1900−1700 cm^{-1}, characteristic of organic carbonyls. These latter IR absorption bands are assigned to C═O-containing byproducts, such as acetic anhydride (whose spectrum is also reported in Figure 5 for comparison), adsorbed on the sample.

Interpretation of the IR absorption bands in the 2000−1900 cm^{-1} region is more difficult, also because they evolve as a function of temperature (an isosbestic point at 1945 cm^{-1} is observed). However, the following considerations can be done: (i) the total intensity of the IR absorption bands in the υ(CO) region is much lower than that observed when CO is used as a probe of the Pd nanoparticles obtained by reducing Pd(II)−polymer in H_2; (ii) the IR absorption bands in the υ(CO) region are very narrow and compatible (at least in part) with those expected for $Pd_4(CO)_4(OAc)_4$ or analogous clusters.[94] The total intensity might be a consequence of the higher adsorption temperature, but also of a minor amount of surface sites available for CO adsorption. A second experiment was performed in order to separate the two effects: after the CO-reduction step, the sample was cooled at room temperature and CO was adsorbed. The new FT-IR spectra (not shown) are

dx.doi.org/10.1021/jp5003897 | J. Phys. Chem. C 2014, 118, 8406−8415

still one order of magnitude less intense than those obtained on the sample reduced in H_2, demonstrating that the accessible surface area is much smaller for Pd nanoparticles obtained in CO. In conclusion, FT-IR spectroscopy in reaction conditions allows simultaneous monitoring of (i) the reduction of palladium acetate, (ii) the formation of C═O-containing byproducts (which are irreversibly adsorbed even after degassing at 160 °C), and (iii) the formation of carbonyl species on Pd clusters, whose nature can vary from Pd(I) acetate clusters to Pd(0) nanoparticles with unclean surfaces.

TEM images (Figure 5b) reveal that the Pd NPs formed upon reducing Pd(II)−polymer in CO are different from those formed in the presence of H_2. In particular, they are larger and show peculiar morphologies, such as triangles and hexagons. These morphologies were observed for both the smaller and bigger particles. In this respect, it has been recently reported that Pd nanoparticles exhibiting unusual triangular shapes are generated when palladacycle complexes or palladium acetate in solution are treated with CO at room temperature.[95] Also CO reduction of Pd(II) compounds in toluene in combination with stabilization by amphiphilic polymers was reported to selectively afford dispersions of hexagonal platelets.[13] The phenomenon observed in our case is similar, although it occurs entirely at the solid/gas interface, and not in solution. It is likely that the observed shapes are specific to the reduction process of palladium acetate with CO, in combination with a polymer (or a solvent) that adsorbs to certain crystal faces and thus promotes specific crystal growth.[13] In conclusion, the DRIFT results shown in Figure 5a suggest that intermediate unstable palladium−carbonyl complexes are involved.

3.3.2. Simultaneous SAXS−XAS Experiment in Reaction Conditions. Figure 6a,e shows the evolution of Pd K-edge XANES spectra and SAXS patterns, simultaneously collected during thermal treatment of Pd(II)−polymer in CO from room temperature (black) to 160 °C (red). The XANES spectra (Figure 6a) evolve as a function of temperature in a way similar to what occurs in the presence of H_2: the starting spectrum, typical of palladium acetate, is gradually transformed into a spectrum characteristic of Pd(0). It is worth noticing that the possible presence of Pd(I) intermediate species cannot be excluded, since the XANES spectra of Pd(I) species usually do not display distinguishable features and are very similar to that of Pd(0).[47] The evolution of features A and B as a function of temperature is shown in Figure 6c,d. Reduction of Pd(II)−polymer occurs in a double step, in fair agreement with the FT-IR results shown in Figure 5a: the reaction is slow during step 1 (below 100 °C), although faster than in the presence of H_2; above 100 °C the reaction is faster, and complete reduction is achieved around 160 °C. A constant growth in the intensity of feature B is observed in the whole temperature region, and the final value is bigger than that observed after reduction of Pd(II)−polymer in H_2. This observation suggests that the final Pd nanoparticles have a bigger size, although a direct extrapolation of the particle dimension from the intensity of the first EXAFS oscillation is not straightforward. As already discussed in previous sections, XANES data are averaged on all the Pd present in the sample; bigger particles contribute to the intensity of feature B more than smaller particles.

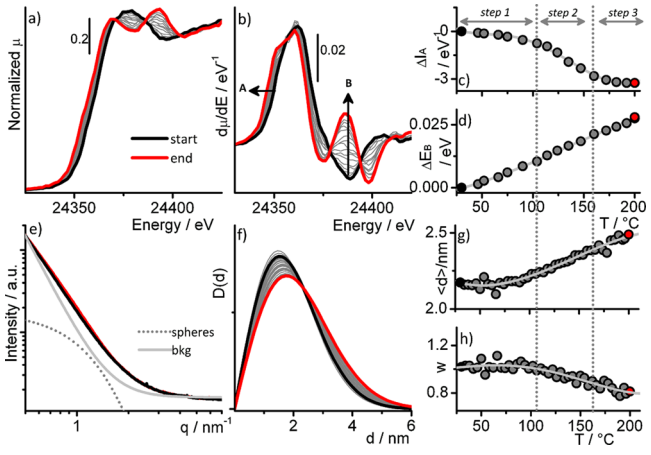

Figure 6. SAXS−XAS data collected simultaneously during reduction of Pd(II)−polymer in CO from room temperature (black) to 200 °C (red); heating rate 2 °C/min. (a and b) Evolution of the normalized XANES spectra and of the derivative signal. Parts c and d show the evolution as a function of temperature of features A (shift in energy) and B (change in intensity) of the derivative XANES spectra (see arrows in part b). (e) SAXS spectra at the beginning (black) and the end (red) of the temperature ramp. Also examples of the theoretical signals obtained by considering a distribution of spherical particles (dotted gray) and the background (gray) are reported. (f) Particle size distribution, (g) average diameter of the Pd particles, and (h) relative weight as a function of temperature, respectively, as obtained from the spherical model fitting of the SAXS data.

The SAXS data collected simultaneously to the XANES spectra are shown in Figure 6e. Also the theoretical curves corresponding to the background (light gray) and to a distribution of spherical particles (dotted) are reported. The evolution of the main structural parameters as a function of temperature, as obtained from the spherical model fitting, are reported in Figure 6g,h. The phenomena observed during transformation of Pd(II)−polymer into Pd(0)−polymer in CO are completely different from those observed in the presence of H_2. In particular, (i) the average particle diameter increases over the whole temperature range, faster during step 2 (Figure 6g), (ii) the particle size distribution becomes broader (Figure 6f), and (iii) the number of particles contributing to the overall $I(q)$ signal decreases (Figure 6h). It is important to observe that, also in this case, since the experimental setup was suited for small particles, SAXS data can reveal only particles smaller than 10 nm in diameter.

4. CONCLUSIONS

Pd NPs were formed inside a porous (highly cross-linked) polystyrene scaffold upon gas-phase reduction of palladium acetate precursor. Gaseous H_2 and CO were used as reducing agents. The process was monitored by means of time-resolved SAXS and XANES techniques, simultaneously applied in reaction conditions, in conjunction with DR UV−vis and DRIFT spectroscopies and TEM measurements. It was found that the reduction process proceeds in two steps in the presence of both H_2 and CO gases, slower below about 100 °C, and faster above. In both cases, complete reduction of palladium acetate is achieved at 160 °C. The reducing agent affects both the speed of palladium acetate reduction and the properties of the obtained Pd NPs. In particular, the following occur:

(i) Reduction of palladium acetate starts at lower temperature (already at room temperature) and proceeds faster in the presence of CO than with H_2.

(ii) The Pd NPs are bigger when formed in CO and show peculiar morphologies (triangles and hexagons), whereas those formed in H_2 are smaller and spherical in shape.

dx.doi.org/10.1021/jp5003897 | J. Phys. Chem. C 2014, 118, 8406−8415

(iii) Pd NPs formed in CO have unclean surfaces, probably as a consequence of residual byproducts (such as acetic anhydride) that are not desorbed at the reduction temperature.

The reason for the different properties of the formed Pd NPs has to be searched for in the different mechanism of palladium acetate reduction. It is likely that, in the presence of CO, Pd acetate carbonyl intermediates are formed, where CO acts as structure-inducing agent, promoting the crystal growth in specific directions. These results might have interesting perspectives in catalysis, since it is well documented that for metal nanoparticles the catalytic reactivity is dependent not only on the size control (and size distribution) but also on the exposure of the right planes.

As a general conclusion, the present work demonstrates that, when dealing with the characterization of metal NPs, most of the employed techniques have some limitations. However, a synergic combination of multiple complementary techniques, possibly applied in reaction conditions, allows overcoming the problems and obtaining a clear picture of the entire process that leads from the metal precursor to metal NPs.[96]

AUTHOR INFORMATION

Corresponding Authors

*E-mail: elena.groppo@unito.it.

*E-mail: alessandro.longo@cnr.it.

Present Address

[#]L.W.: State Key Laboratory of Hollow-fiber Membrane Materials and Membrane Processes, School of Environmental and Chemical Engineering, Tianjin Polytechnic University, Tianjin 300387, People's Republic of China.

Funding

The BM26 staff is acknowledged for the technical support. This work has been supported by "Progetti di Ricerca di Ateneo-Compagnia di San Paolo-2011- Linea 1", ORTO11RRT5 project. C.L. thanks the support from the Mega-grant of the Russian Federation Government to support scientific research at Southern Federal University, No.14.Y26.31.0001.

Notes

The authors declare no competing financial interest.

ACKNOWLEDGMENTS

Lauren Adams is kindly acknowledged for her contribution to the DRIFT measurements.

REFERENCES

(1) Blaser, H.-U.; Indolese, A.; Schnyder, A.; Steiner, H.; Studer, M. Supported Palladium Catalysts For Fine Chemicals Synthesis. *J. Mol. Catal. A: Chem.* **2001**, *173*, 3−18.

(2) Pernicone, N.; Cerboni, M.; Prelazzi, G.; Pinna, F.; Fagherazzi, G. An Investigation On Pd/C Industrial Catalysts For The Purification Of Terephthalic Acid. *Catal. Today* **1998**, *44*, 129−135.

(3) Duca, D.; Arena, F.; Parmaliana, A.; Deganello, G. Hydrogenation Of Acetylene In Ethylene Rich Feedstocks: Comparison Between Palladium Catalysts Supported On Pumice And Alumina. *Appl. Catal., A* **1998**, *172*, 207−216.

(4) Figueras, F.; Coq, B. Hydrogenation And Hydrogenolysis Of Nitro-, Nitroso-, Azo-, Azoxy- And Other Nitrogen-Containing Compounds On Palladium. *J. Mol. Catal. A: Chem.* **2001**, *173*, 223−230.

(5) Santacesaria, E.; Wilkinson, P.; Babini, P.; Carra, S. Hydrogenation Of 2-Ethyltetrahydroanthraquinone In The Presence Of Palladium Catalyst. *Ind. Eng. Chem. Res.* **1988**, *27*, 780−784.

(6) Studer, M.; Blaser, H. U. Influence Of Catalyst Type, Solvent, Acid And Base On The Selectivity And Rate In The Catalytic Debenzylation Of 4-Chloro-N,N-Dibenzyl Aniline With Pd/C And H-2. *J. Mol. Catal. A: Chem.* **1996**, *112*, 437−445.

(7) Groppo, E.; Agostini, G.; Piovano, A.; Muddada, N. B.; Leofanti, G.; Pellegrini, R.; Portale, G.; Longo, A.; Lamberti, C. Effect Of Reduction In Liquid Phase On The Properties And The Catalytic Activity Of Pd/Al2O3 Catalysts. *J. Catal.* **2012**, *287*, 44−54.

(8) Shenhar, R.; Norsten, T. B.; Rotello, V. M. Polymer-Mediated Nanoparticle Assembly: Structural Control And Applications. *Adv. Mater.* **2005**, *17*, 657−669.

(9) Pathak, S.; Greci, M. T.; Kwong, R. C.; Mercado, K.; Prakash, G. K. S.; Olah, G. A.; Thompson, M. E. Synthesis And Applications Of Palladium-Coated Poly(Vinylpyridine) Nanospheres. *Chem. Mater.* **2000**, *12*, 1985−1989.

(10) Seregina, M. V.; Bronstein, L. M.; Platonova, O. A.; Chernyshov, D. M.; Valetsky, P. M.; Hartmann, J.; Wenz, E.; Antonietti, M. Preparation Of Noble-Metal Colloids In Block Copolymer Micelles And Their Catalytic Properties In Hydrogenation. *Chem. Mater.* **1997**, *9*, 923−931.

(11) Klingelhofer, S.; Heitz, W.; Greiner, A.; Oestreich, S.; Forster, S.; Antonietti, M. Preparation Of Palladium Colloids In Block Copolymer Micelles And Their Use For The Catalysis Of The Heck Reaction. *J. Am. Chem. Soc.* **1997**, *119*, 10116−10120.

(12) Bronstein, L. M.; Chernyshov, D. M.; Volkov, I. O.; Ezernitskaya, M. G.; Valetsky, P. M.; Matveeva, V. G.; Sulman, E. M. Structure And Properties Of Bimetallic Colloids Formed In Polystyrene-Block-Poly-4-Vinylpyridine Micelles: Catalytic Behavior In Selective Hydrogenation Of Dehydrolinalool. *J. Catal.* **2000**, *196*, 302−314.

(13) Schlotterbeck, U.; Aymonier, C.; Thomann, R.; Hofmeister, H.; Tromp, M.; Richtering, W.; Mecking, S. Shape-Selective Synthesis Of Palladium Nanoparticles Stabilized By Highly Branched Amphiphilic Polymers. *Adv. Funct. Mater.* **2004**, *14*, 999−1004.

(14) Okamoto, K.; Akiyama, R.; Yoshida, H.; Yoshida, T.; Kobayashi, S. Formation Of Nanoarchitectures Including Subnanometer Palladium Clusters And Their Use As Highly Active Catalysts. *J. Am. Chem. Soc.* **2005**, *127*, 2125−2135.

(15) Akiyama, R.; Kobayashi, S. "Microencapsulated" And Related Catalysts For Organic Chemistry And Organic Synthesis. *Chem. Rev.* **2009**, *109*, 594−642.

(16) Akiyama, R.; Kobayashi, S. The Polymer Incarcerated Method For The Preparation Of Highly Active Heterogeneous Palladium Catalysts. *J. Am. Chem. Soc.* **2003**, *125*, 3412−3413.

(17) Akiyama, R.; Kobayashi, S. A Novel Polymer-Supported Arene-Ruthenium Complex For Ring-Closing Olefin Metathesis. *Angew. Chem., Int. Ed.* **2002**, *41*, 2602−2604.

(18) Akiyama, R.; Kobayashi, S. Microencapsulated Palladium Catalysts: Allylic Substitution And Suzuki Coupling Using A Recoverable And Reusable Polymer-Supported Palladium Catalyst. *Angew. Chem., Int. Ed.* **2001**, *40*, 3469−3471.

(19) Kobayashi, S.; Akiyama, R. Renaissance Of Immobilized Catalysts. New Types Of Polymer-Supported Catalysts, 'Microencapsulated Catalysts', Which Enable Environmentally Benign And Powerful High-Throughput Organic Synthesis. *Chem. Commun.* **2003**, 449−460.

(20) Dioos, B. M. L.; Vankelecom, I. F. J.; Jacobs, P. A. Aspects Of Immobilisation Of Catalysts On Polymeric Supports. *Adv. Synth. Catal.* **2006**, *348*, 1413−1446.

(21) Hodge, P. Polymer-Supported Organic Reactions: What Takes Place In The Beads? *Chem. Soc. Rev.* **1997**, *26*, 417−424.

(22) Barbaro, P. Recycling Asymmetric Hydrogenation Catalysts By Their Immobilization Onto Ion-Exchange Resins. *Chem.—Eur. J.* **2006**, *12*, 5666−5675.

(23) Moreno-Marrodan, C.; Barbaro, P.; Catalano, M.; Taurino, A. Green Production Of Polymer-Supported PdNPs: Application To The Environmentally Benign Catalyzed Synthesis Of cis-3-Hexen-1-ol Under Flow Conditions. *Dalton Trans.* **2012**, *41*, 12666−12669.

(24) Ott, L. S.; Finke, R. G. Transition-Metal Nanocluster Stabilization For Catalysis: A Critical Review Of Ranking Methods And Putative Stabilizers. *Coord. Chem. Rev.* **2007**, *251*, 1075−1100.

(25) Corain, B.; Jerabek, K.; Centomo, P.; Canton, P. Generation Of Size-Controlled Pd-0 Nanoclusters Inside Nanoporous Domains Of Gel-Type Resins: Diverse And Convergent Evidence That Supports A Strategy Of Template-Controlled Synthesis. *Angew. Chem., Int. Ed.* **2004**, *43*, 959−962.
(26) Roucoux, A.; Schulz, J.; Patin, H. Reduced Transition Metal Colloids: A Novel Family Of Reusable Catalysts? *Chem. Rev.* **2002**, *102*, 3757−3778.
(27) Bonnemann, H.; Richards, R. M. Nanoscopic Metal Particles—Synthetic Methods And Potential Applications. *Eur. J. Inorg. Chem.* **2001**, 2455−2480.
(28) Pan, C.; Pelzer, K.; Philippot, K.; Chaudret, B.; Dassenoy, F.; Lecante, P.; Casanove, M. J. Ligand-Stabilized Ruthenium Nanoparticles: Synthesis, Organization, And Dynamics. *J. Am. Chem. Soc.* **2001**, *123*, 7584−7593.
(29) Dahl, J. A.; Maddux, B. L. S.; Hutchison, J. E. Toward Greener Nanosynthesis. *Chem. Rev.* **2007**, *107*, 2228−2269.
(30) Groppo, E.; Liu, W.; Zavorotynska, O.; Agostini, G.; Spoto, G.; Bordiga, S.; Lamberti, C.; Zecchina, A. Subnanometric Pd Particles Stabilized Inside Highly Cross-Linked Polymeric Supports. *Chem. Mater.* **2010**, *22*, 2297−2308.
(31) Xia, Y. N.; Xiong, Y. J.; Lim, B.; Skrabalak, S. E. Shape-Controlled Synthesis Of Metal Nanocrystals: Simple Chemistry Meets Complex Physics? *Angew. Chem., Int. Ed.* **2009**, *48*, 60−103.
(32) Wang, R.; He, H.; Liu, L. C.; Dai, H. X.; Zhao, Z. Shape-Dependent Catalytic Activity Of Palladium Nanocrystals For The Oxidation Of Carbon Monoxide. *Catal. Sci. Technol.* **2012**, *2*, 575−580.
(33) Abecassis, B.; Testard, F.; Spalla, O.; Barboux, P. Probing In Situ The Nucleation And Growth Of Gold Nanoparticles By Small-Angle X-Ray Scattering. *Nano Lett.* **2007**, *7*, 1723−1727.
(34) Harada, M.; Inada, Y.; Nomura, M. In Situ Time-Resolved XAFS Analysis Of Silver Particle Formation By Photoreduction In Polymer Solutions. *J. Colloid Interface Sci.* **2009**, *337*, 427−438.
(35) Harada, M.; Tamura, N.; Takenaka, M. Nucleation And Growth Of Metal Nanoparticles During Photoreduction Using In Situ Time-Resolved SAXS Analysis. *J. Phys. Chem. C* **2011**, *115*, 14081−14092.
(36) Harada, M.; Katagiri, E. Mechanism Of Silver Particle Formation During Photoreduction Using In Situ Time-Resolved SAXS Analysis. *Langmuir* **2010**, *26*, 17896−17905.
(37) Sakamoto, N.; Harada, M.; Hashimoto, T. In Situ And Time-Resolved SAXS Studies Of Pd Nanoparticle Formation In A Template Of Block Copolymer Microdomain Structures. *Macromolecules* **2006**, *39*, 1116−1124.
(38) Tanaka, H.; Koizumi, S.; Hashimoto, T.; Itoh, H.; Satoh, M.; Naka, K.; Chujo, Y. Combined In Situ And Time-Resolved SANS And SAXS Studies Of Chemical Reactions At Specific Sites And Self-Assembling Processes Of Reaction Products: Reduction Of Palladium Ions In Self-Assembled Polyamidoamine Dendrimers As A Template. *Macromolecules* **2007**, *40*, 4327−4337.
(39) Zhao, Y.; Saijo, K.; Takenaka, M.; Koizumi, S.; Hashimoto, T. Time-Resolved SAXS Studies Of Self-Assembling Process Of Palladium Nanoparticles In Templates Of Polystyrene-Block-Polyisoprene Melt: Effects Of Reaction Fields On The Self-Assembly. *Polymer* **2009**, *50*, 2696−2705.
(40) Harada, M.; Inada, Y. In Situ Time-Resolved XAFS Studies Of Metal Particle Formation By Photoreduction In Polymer Solutions. *Langmuir* **2009**, *25*, 6049−6061.
(41) Abecassis, B.; Testard, F.; Kong, Q. Y.; Francois, B.; Spalla, O. Influence Of Monomer Feeding On A Fast Cold Nanoparticles Synthesis: Time-Resolved XANES And SAXS Experiments. *Langmuir* **2010**, *26*, 13847−13854.
(42) Polte, J.; Ahner, T. T.; Delissen, F.; Sokolov, S.; Emmerling, F.; Thunemann, A. F.; Kraehnert, R. Mechanism Of Gold Nanoparticle Formation In The Classical Citrate Synthesis Method Derived From Coupled In Situ XANES And SAXS Evaluation. *J. Am. Chem. Soc.* **2010**, *132*, 1296−1301.
(43) Horiuchi, S.; Sarwar, M. I.; Nakao, Y. Nanoscale Assembly Of Metal Clusters In Block Copolymer Films With Vapor Of A Metal-Acetylacetonato Complex Using A Dry Process. *Adv. Mater.* **2000**, *12*, 1507−1511.
(44) Newton, M. A.; Van Beek, W. Combining Synchrotron-Based X-Ray Techniques With Vibrational Spectroscopies For The In Situ Study Of Heterogeneous Catalysts: A View From A Bridge. *Chem. Soc. Rev.* **2010**, *39*, 4845−4863.
(45) Newton, M. A.; Di Michiel, M.; Kubacka, A.; Fernandez-Garcia, M. Combining Time-Resolved Hard X-Ray Diffraction And Diffuse Reflectance Infrared Spectroscopy To Illuminate CO Dissociation And Transient Carbon Storage By Supported Pd Nanoparticles During CO/NO Cycling. *J. Am. Chem. Soc.* **2010**, *132*, 4540−4541.
(46) Newton, M. A. Dynamic Adsorbate/Reaction Induced Structural Change Of Supported Metal Nanoparticles: Heterogeneous Catalysis And Beyond. *Chem. Soc. Rev.* **2008**, *37*, 2644−2657.
(47) Iglesias-Juez, A.; Kubacka, A.; Fernandez-Garcia, M.; Di Michiel, M.; Newton, M. A. Nanoparticulate Pd Supported Catalysts: Size-Dependent Formation Of Pd(I)/Pd(0) And Their Role In CO Elimination. *J. Am. Chem. Soc.* **2011**, *133*, 4484−4489.
(48) Agostini, G.; Lamberti, C.; Pellegrini, R.; Leofanti, G.; Giannici, F.; Longo, A.; Groppo, E. Effect Of Pre-Reduction On The Properties And The Catalytic Activity Of Pd/Carbon Catalysts: A Comparison With Pd/Al_2O_3. *ACS Catal.* **2014**, *4*, 187−194.
(49) Groppo, E.; Bertarione, S.; Rotunno, F.; Agostini, G.; Scarano, D.; Pellegrini, R.; Leofanti, G.; Zecchina, A.; Lamberti, C. Role Of The Support In Determining The Vibrational Properties Of Carbonyls Formed On Pd Supported On SiO_2-Al_2O_3, Al_2O_3, And MgO. *J. Phys. Chem. C* **2007**, *111*, 7021−7028.
(50) Agostini, G.; Groppo, E.; Piovano, A.; Pellegrini, R.; Leofanti, G.; Lamberti, C. Preparation Of Pd Supported Catalysts: From The Pd-Precursor Solution To The Deposited Pd^{2+} Phase. *Langmuir* **2010**, *26*, 11204−11211.
(51) Agostini, G.; Pellegrini, R.; Leofanti, G.; Bertinetti, L.; Bertarione, S.; Groppo, E.; Zecchina, A.; Lamberti, C. Determination Of The Particle Size, Available Surface Area, And Nature Of Exposed Sites For Silica-Alumina-Supported Pd Nanoparticles: A Multi-technical Approach. *J. Phys. Chem. C* **2009**, *113*, 10485−10492.
(52) Pellegrini, R.; Leofanti, G.; Agostini, G.; Bertinetti, L.; Bertarione, S.; Groppo, E.; Zecchina, A.; Lamberti, C. Influence Of K-Doping On A Pd/SiO2−Al2O3 Catalyst. *J. Catal.* **2009**, *267*, 40−49.
(53) Groppo, E.; Uddin, M. J.; Zavorotynska, O.; Damin, A.; Vitillo, J. G.; Spoto, G.; Zecchina, A. Exploring The Chemistry Of Electron Accepting Molecules In The Cavities Of The Basic Microporous P4VP Polymer By In Situ FTIR Spectroscopy. *J. Phys. Chem. C* **2008**, *112*, 19493−19500.
(54) Lamberti, C.; Zecchina, A.; Groppo, E.; Bordiga, S. Probing The Surfaces Of Heterogeneous Catalysts By In Situ IR Spectroscopy. *Chem. Soc. Rev.* **2010**, *39*, 4951−5001.
(55) Ozensoy, E.; Goodman, D. W. Vibrational Spectroscopic Studies On CO Adsorption, NO Adsorption CO Plus NO Reaction On Pd Model Catalysts. *Phys. Chem. Chem. Phys.* **2004**, *6*, 3765−3778.
(56) Henry, C. R. Surface Studies Of Supported Model Catalysts. *Surf. Sci. Rep.* **1998**, *31*, 235−325.
(57) Bertarione, S.; Scarano, D.; Zecchina, A.; Johanek, V.; Hoffmann, J.; Schauermann, S.; Frank, M. M.; Libuda, J.; Rupprechter, G.; Freund, H. J. Surface Reactivity Of Pd Nanoparticles Supported On Polycrystalline Substrates As Compared To Thin Film Model Catalysts: Infrared Study Of CO Adsorption. *J. Phys. Chem. B* **2004**, *108*, 3603−3613.
(58) Bertarione, S.; Prestipino, C.; Groppo, E.; Scarano, D.; Spoto, G.; Zecchina, A.; Pellegrini, R.; Leofanti, G.; Lamberti, C. Direct IR Observation Of Vibrational Properties Of Carbonyl Species Formed On Pd Nano-Particles Supported On Amorphous Carbon: Comparison With Pd/SiO_2-Al_2O_3. *Phys. Chem. Chem. Phys.* **2006**, *8*, 3676−3681.
(59) Lear, T.; Marshall, R.; Lopez-Sanchez, J. A.; Jackson, S. D.; Klapotke, T. M.; Baumer, M.; Rupprechter, G.; Freund, H. J.; Lennon, D. The Application Of Infrared Spectroscopy To Probe The Surface

Morphology Of Alumina-Supported Palladium Catalysts. *J. Chem. Phys.* **2005**, *123*, No. 174706.
(60) Lear, T.; Marshall, R.; Gibson, E. K.; Schutt, T.; Klapotke, T. M.; Rupprechter, G.; Freund, H. J.; Winfield, J. M.; Lennon, D. A Model High Surface Area Alumina-Supported Palladium Catalyst. *Phys. Chem. Chem. Phys.* **2005**, *7*, 565−567.
(61) Longo, A.; Portale, G.; Bras, W.; Giannici, F.; Ruggirello, A. M.; Turco Liveri, V. Structural Characterization Of Frozen n-Heptane Solutions Of metal-Containing Reverse Micelles. *Langmuir* **2007**, *23*, 11482−11487.
(62) Nikitenko, S.; Beale, A. M.; Van Der Eerden, A. M. J.; Jacques, S. D. M.; Leynaud, O.; O'Brien, M. G.; Detollenaere, D.; Kaptein, R.; Weckhuysen, B. M.; Bras, W. Implementation Of A Combined SAXS/WAXS/QEXAFS Set-Up For Time-Resolved In Situ Experiments. *J. Synchrotron Radiat.* **2008**, *15*, 632−640.
(63) Ravel, B.; Newville, M. ATHENA, ARTEMIS, HEPHAESTUS: Data Analysis For X-Ray Absorption Spectroscopy Using IFEFFIT. *J. Synchrotron Radiat.* **2005**, *12*, 537−541.
(64) Hammersley, A. P.; Svensson, S. O.; Hanfland, M.; Fitch, A. N.; Häusermann, D. *High Pressure Res.* **1996**, *14*, 235−248.
(65) Bradley, J. S. In *Clusters And Colloids: From Theory To Applications*; Schmid, G., Ed.; VCH: Weinheim, Germany, 1994; p 459.
(66) *Nanoparticles: From Theory To Application*; Schmid, G., Ed.; Wiley-VCH: Weinheim, Germany, 2004.
(67) *Metal Nanoparticles: Synthesis, Characterization And Applications*; Feldheim, D. L., Foss, C. A., Eds.; Marcel Dekker: New York, 2002.
(68) Moiseev, I. I.; Stromnova, T. A.; Vargaftik, M. N.; Mazo, G. J.; Kuz'mina, L. G.; Struchkov, Y. T. New Palladium Carbonyl Clusters: X-Ray Crystal Structure Of [Pd4(CO)4(OAc)4](AcOH)2. *J. Chem. Soc., Chem. Commun.* **1978**, 27−28.
(69) Moiseev, I. I. Pd-4 Clusters—The Sensitivity Of The Cluster Metal Core Geometry To The Surrounding Ligands. *J. Organomet. Chem.* **1995**, *488*, 183−190.
(70) Stromnova, T. A.; Moiseev, I. I. Palladium Carbonyl Complexes. *Usp. Khim.* **1998**, *67*, 542−572.
(71) Stromnova, T. A.; Moiseev, I. I. Palladium(I) Carbonyl Complexes. *Russ. J. Coord. Chem.* **1998**, *24*, 227−241.
(72) Stromnova, T. A.; Shishilov, O. N.; Dayneko, M. V.; Monakhov, K. Y.; Churakov, A. V.; Kuz'mina, L. G.; Howard, J. A. K. Palladium(I) Carbonyl Carboxylate Clusters Cyclo-[Pd-2(Mu-CO)(2)(Mu-OCOR)(2)](N) (N=2 Or 3): Structure And Reactivity. *J. Organomet. Chem.* **2006**, *691*, 3730−3736.
(73) Moiseev, I. I.; Stromnova, T. A.; Vargaftik, M. N. Low-Valence Palladium Complexes: Stoichiometric Reactions And Catalysis. *Russ. Chem. Bull.* **1998**, *47*, 777−785.
(74) Kragten, D. D.; Van Santen, R. A.; Crawford, M. K.; Provine, W. D.; Lerou, J. J. A Spectroscopic Study Of The Homogeneous Catalytic Conversion Of Ethylene To Vinyl Acetate By Palladium Acetate. *Inorg. Chem.* **1999**, *38*, 331−339.
(75) Pandey, R. N.; Henry, P. M. Interaction Of Palladium(II) Acetate With Sodium And Lithium Acetate In Acetic Acid. *Can. J. Chem.* **1974**, *52*, 1241−1247.
(76) Wang, J.; Boelens, H. F. M.; Thathagar, M. B.; Rothenberg, G. In Situ Spectroscopic Analysis Of Nanocluster Formation. *ChemPhysChem* **2004**, *5*, 93−98.
(77) Gaikwad, A. V.; Rothenberg, G. In-Situ UV-Visible Study Of Pd Nanocluster Formation In Solution. *Phys. Chem. Chem. Phys.* **2006**, *8*, 3669−3675.
(78) Xiong, Y. J.; Chen, J. Y.; Wiley, B.; Xia, Y. N.; Yin, Y. D.; Li, Z. Y. Size-Dependence Of Surface Plasmon Resonance And Oxidation For Pd Nanocubes Synthesized Via A Seed Etching Process. *Nano Lett.* **2005**, *5*, 1237−1242.
(79) Evanoff, D. D.; Chumanov, G. Synthesis And Optical Properties Of Silver Nanoparticles And Arrays. *ChemPhysChem* **2005**, *6*, 1221−1231.
(80) Evanoff, D. D.; Chumanov, G. Size-Controlled Synthesis Of Nanoparticles. 2. Measurement Of Extinction, Scattering, And Absorption Cross Sections. *J. Phys. Chem. B* **2004**, *108*, 13957−13962.
(81) Stoyanov, E. IR Study Of The Structure Of Palladium(II) Acetate In Chloroform, Acetic Acid, And Their Mixtures In Solution And In Liquid-Solid Subsurface Layers. *J. Struct. Chem.* **2000**, *41*, 440−445.
(82) Stephenson, T. A.; Wilkinson, G. Acetato Complexes Of Palladium(II). *J. Inorg. Nucl. Chem.* **1967**, *29*, 2122−2123.
(83) Nakamoto, K. *Infrared And Raman Spectra Of Inorganic And Coordination Compounds*; John Wiley & Sons: New York, 2006.
(84) Bradley, J. S.; Hill, E. W.; Behal, S.; Klein, C.; Chaudret, B.; Duteil, A. Preparation And Characterization Of Organosols Of Monodispersed Nanoscale Palladium—Particle-Size Effects In The Binding Geometry Of Adsorbed Carbon-Monoxide. *Chem. Mater.* **1992**, *4*, 1234−1239.
(85) Bradley, J. S.; Millar, J. M.; Hill, E. W.; Behal, S. Surface-Chemistry On Transition-Metal Colloids—An Infrared And NMR-Study Of Carbon-Monoxide Adsorption On Colloidal Platinum. *J. Catal.* **1991**, *129*, 530−539.
(86) Sheu, L. L.; Karpinski, Z.; Sachtler, W.-M. H. Effects Of Palladium Particle Size And Palladium Silicide Formation On Fourier Transform Infrared Spectra And Carbon Monoxide Adsorbed On Palladium/Silicon Dioxide Catalysts. *J. Phys. Chem.* **1989**, *93*, 4890−4894.
(87) Sheu, L.-L.; Knözinger, H.; Sachtler, W. M. H. Palladium Carbonyl Clusters Entrapped In NaY Zeolite Cages: Ligand Dissociation And Cluster-Wall Interactions. *J. Am. Chem. Soc.* **1989**, *111*, 8121−8131.
(88) Tessier, D.; Rakai, A.; Bozonverduraz, F. Spectroscopic Study Of The Interaction Of Carbon-Monoxide With Cationic And Metallic Palladium In Palladium Alumina Catalysts. *J. Chem. Soc., Faraday Trans.* **1992**, *88*, 741−749.
(89) Perez-Osorio, G.; Castillon, F.; Simakov, A.; Tiznado, H.; Zaera, F.; Fuentes, S. Effect Of Ceria-Zirconia Ratio On The Interaction Of CO With PdO/Al2O3-(Ce-X-Zr1-X)O-2 Catalysts Prepared By Sol-Gel Method. *Appl. Catal., B: Environ.* **2007**, *69*, 219−225.
(90) Zhu, H. Q.; Qin, Z. F.; Shan, W. J.; Shen, W. J.; Wang, J. G. Low-Temperature Oxidation Of CO Over Pd/CeO2-TiO2 Catalysts With Different Pretreatments. *J. Catal.* **2005**, *233*, 41−50.
(91) Tiznado, H.; Fuentes, S.; Zaera, F. Infrared Study Of CO Adsorbed On Pd/Al2O3-ZrO2. Effect Of Zirconia Added By Impregnation. *Langmuir* **2004**, *20*, 10490−10497.
(92) Moller, K.; Bein, T. Reduction And Cluster Growth Of Palladium In Zeolite-Y Containing Transition-Metal Ions—X-Ray Absorption Studies. *J. Phys. Chem.* **1990**, *94*, 845−853.
(93) Zhang, Z. C.; Chen, H. Y.; Sachtler, W. M. H. Migration And Coalescence Of Pd Carbonyl Clusters In Zeolite-Y. *J. Chem. Soc., Faraday Trans.* **1991**, *87*, 1413−1418.
(94) Stephenson, T. A.; Morehouse, S. M.; Powell, A. R.; Heffer, J. P.; Wilkinson, G. Carboxylates Of Palladium, Platinum, And Rhodium, And Their Adducts. *J. Chem. Soc.* **1965**, 3632−3640.
(95) Grigg, R.; Zhang, L. X.; Collard, S.; Ellis, P.; Keep, A. Facile Generation And Morphology Of Pd Nanoparticles From Palladacycles And Carbon Monoxide. *J. Organomet. Chem.* **2004**, *689*, 170−173.
(96) Bordiga, S.; Groppo, E.; Agostini, G.; van Bokhoven, J. A.; Lamberti, C. Reactivity of Surface Species in Heterogeneous Catalysts Probed by In Situ X-ray Absorption Techniques. *Chem. Rev.* **2013**, *113*, 1736−1850.